JOURNAL OF GUIDANCE, CONTROL, AND DYNAMICS
Vol. 25, No. 3, May–June 2002

Incremental-Angle and Angular Velocity Estimation Using a Star Sensor

G. Nagendra Rao and T. K. Alex
Indian Space Research Organization, Bangalore 560 058, India
and
M. Seetharama Bhat
Indian Institute of Science, Bangalore 560 018, India

A method is described for estimating the incremental angle and angular velocity of a spacecraft using integrated rate parameters with the help of a star sensor alone. The chief advantage of this method is that the measured stars need not be identified, whereas the identification of the stars is necessary in earlier methods. This proposed estimation can be carried out with all of the available measurements by a simple linear Kalman filter, albeit with a time-varying sensitivity matrix. The residuals of estimated angular velocity by the proposed spacecraft incremental-angle and angular velocity estimation method are as accurate as the earlier methods. This method also enables the spacecraft attitude to be reconstructed for mapping the stars into an imaginary unit sphere in the body reference frame, which will preserve the true angular separation of the stars. This will pave the way for identification of the stars using any angular separation or triangle matching techniques applied to even a narrow field of view sensor that is made to sweep the sky. A numerical simulation for inertial as well as Earth pointing spacecraft is carried out to establish the results.

Introduction

STAR trackers are the most accurate instruments available to spacecraft designers for attitude determination and payload pointing.[1] Yet, there are not many spacecraft that are equipped with only star trackers as primary sensors. Generally either magnetometer, Earth sensor, sun sensor, and, more recently, global positioning

Goparaju Nagendra Rao obtained his Bachelor of Technology degree in 1979 from Sri Venkateswara University, Tirupathi, and Master of Engineering degree from the Indian Institute of Science in 1981. He worked on image processing for smart sensors and linear charge-coupled-device-array-based star mappers for IRS-1A/1B satellites. He developed area-array-based star trackers for Indian Remote Sensing IRS-1C, IRS-1D, and IRS-P3 spacecraft. He designed a miniature star sensor for the GSAT-I spacecraft. His specialization is in the development of microprocessor and digital-signal-processor-based instruments for the spacecraft. He currently heads a division in the Laboratory for Electro-Optics Systems, a unit of the Indian Space Research Organization, and pursues the research program in the Aerospace Engineering Department, Indian Institute of Science; gnrao@blr.vsnl.net.in

T. K. Alex received his Bachelor of Science degree in Engineering from Kerala University, his Master of Technology in Instrumentation from the Indian Institute of Technology, Madras, and his Ph.D. from the Indian Institute of Science, Bangalore. At present, he is the director of the Laboratory for Electro-Optics Systems of the Indian Space Research Organization, Bangalore. He is responsible for the development of different types of attitude sensors flown on all Indian satellites. He is a fellow of the Indian National Academy of Engineering and a fellow of the Institution of Electronics and Telecommunication Engineering, India. His main areas of research are electro-optic sensors, instrumentation, and optical systems for imaging payloads in satellites; tkalex@vsnl.com

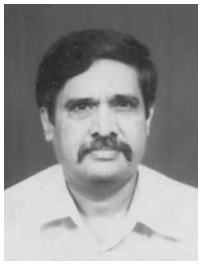

M. Seetharama Bhat obtained his Bachelor and Master of Engineering, and Ph.D. degrees from the Indian Institute of Science, Bangalore (1975, 1977, and 1982). He is currently a professor in the Aerospace Engineering Department, the Indian Institute of Science. Seetharama Bhat deals with dynamics, navigation, guidance, and control of aerospace vehicles, smart laminated beam and plate structures, and thrust vector control for highly maneuverable aircraft. His research activities include the development of control and instrumentation for microair vehicles, satellite orbit and attitude estimation using global positioning systems and star sensors, optimal explicit closed-loop guidance for a multistage launch vehicle, H_∞ optimal control, robust eigenstructure assignment, and variable structure control; msbdcl@aero.iisc.ernet.in

Received 11 April 2001; revision received 4 September 2001; accepted for publication 25 October 2001.

system, or a combination thereof is used for the spacecraft coarse attitude acquisition phase. Subsequently, during the normal mode of operation, rate integrating gyros (RIG) are generally used for attitude feedback control. These sensors suffer from drift, noise, and life-related problems, therefore, accurate spacecraft attitude estimation and control may not always be possible. On the other hand, star observation patterns from the star tracker are matched to their catalog,[2] and accurate instantaneous attitude is estimated using a least-square technique[3] or an extended Kalman filter (EKF). These attitude estimates can be used to periodically correct the drift of the gyroscopes apart from controlling the imaging instruments.[4]

With the advent of microsatellites, the luxury of having dedicated inertial rate sensors in the spacecraft is fast disappearing. Several researchers[5–9] have investigated the possibility of functionally replacing the gyroscopes on the spacecraft by providing the derived attitude rate from the vector observations of sensors such as magnetometer, star tracker, and so on. If an efficient algorithm for attitude and rate estimation using a star tracker can be developed, then it is possible to use the star tracker as the primary spacecraft sensor, with the added advantage of high accuracy.

In the method proposed in Refs. 6, 8, and 9 to derive the spacecraft rate, temporal derivatives of vector measurements are used. These methods suffer from the amplification of noise from the differentiation of noisy temporal measurements. In addition, the knowledge of the matrix that transforms vectors from the reference to the body coordinates (inertial attitude matrix) is required. Also, the reference vector (such as the expected magnetic field direction) at the measured time instant must be known. These conditions cannot be easily met in the case of data from a star tracker. Initially without the help of other coarse attitude sensors, it is not known which part of the sky the star tracker is looking at, and hence, it may not be possible to match the star observations with reference vectors in the star catalog.

In the method described in Refs. 5 and 7, the measured and corresponding reference vector pairs are used for computing the spacecraft attitude and attitude rate using an EKF by linearizing the nonlinear measurement equations. The difficulty in using these methods is that the star pair matching without an a priori attitude knowledge is very difficult, apart from the well-known convergence problems of the EKF if the solution lies far from the initial guess.

In this context, several researchers solve the star identification problem (lost in space) by increasing the field of view (FOV) of the tracker for identifying the star patterns and using an indexed star separation database.[10] Note that, for wide FOV star trackers, the instantaneous measurement accuracy of the tracker is poor.[11] However, when the tracker has a narrow FOV, for example, 8×8 deg, the star pair angular matching technique cannot be applied with ease because of onboard memory constraints due to the requirement of the large number of catalog stars and the associated large star separation database.[12] This is due to the requirement that at least three or more stars need to be seen in the FOV simultaneously, and to achieve this, the tracker needs to look at very faint stars. As the visual magnitude increases, there are more such stars in the celestial sky that need to be stored in the onboard catalog. Reference 13 also illustrates this point, with a huge onboard memory requirement of 24 MB for star identification using a 2×2 deg FOV. In addition, this method may lead to false star identification because the measured star pattern corrupted by noise has to be resolved among many such closely matching patterns stored onboard. This increases the computation overhead.

To mitigate these problems in the star identification process, several authors have tried to use multiple frame star observations while using the spacecraft angular history between the star observations.[14,15] Traditionally gyroscopes are used to compute the spacecraft angle history. This creates a vicious circle. To derive angular rate from the vector observations, the star measurements need to be identified from a reference catalog, and to carry out exactly this star identification process, one needs to know the spacecraft angular rate. Thus, the gyroscope becomes indispensable, which is against the theme of this paper.

This paper attempts to break this circle, by deriving the angular history using only temporal derivatives of the vector measurements without the use of reference or catalog. When the estimated incremental angle is used, the attitude of the spacecraft is reconstructed. With this attitude, the successive measurements are transformed using a recursive average estimate onto a unit sphere in the body frame coordinates. Thus, a star map is derived with respect to an arbitrary epoch. This map is used as a reference subsequently for deriving the improved incremental angle estimates. Also, the generated star map can be used to identify the measured stars and to derive the absolute inertial attitude by applying any of the star identification techniques.[16] Thus, the incremental angle similar to one provided by a rate integrating gyroscope, as well as the absolute attitude seen by the star tracker, can be obtained by star tracker measurements alone. This proposal is the spacecraft incremental-angle and angular velocity estimation (SIAVE) method.

In the development of this method, the spacecraft motion represented using the integrated rate parameters (IRP) described by Oshman and Markley[5] is used. This method uses a higher-order kinematic modeling, which gives a better accuracy compared to earlier methods,[6,7] even when the spacecraft angular velocity is time varying. This feature assumes importance because present day spacecraft (IKONOS, etc.) are highly agile, as they carry out fast maneuvers to point the imaging payload. Oshman and Markley[5] carry out this feat without using the uncertain spacecraft inertia data used earlier by Azor et al.[8] and Harman and Bar-Itzhack.[9] Also, the chosen state vector parameters in this method directly represent the incremental angle and its time derivatives, which are sought to be determined. Hence, this paper banks on the rich theory developed in Ref. 5. Only the equations required to explain the present method are given, wherever necessary.

In contrast to earlier methods given in literature, the proposed method estimates the incremental angle similar to a RIG with a star tracker alone, in addition to the estimation of the angular rate and angular acceleration of the spacecraft. Use of the differences of the current measured directions with the previous estimated directions of the stars minimizes the noise effects unlike the methods of subtracting the temporal measurements. Unlike the previous methods, no onboard star catalog for the estimation of incremental angle and angular rate is required. In a significant deviation, the measurement model is formulated as a linear model, unlike the nonlinear model proposed in Refs. 5 and 7. This helps in a faster and guaranteed convergence of the estimator, which is a very important requirement of any onboard control system. This method provides an auxiliary star map that can be used for identification of the measured star pattern with a reduced star catalog in onboard memory.

A numerical simulation is carried out to establish the results in two cases of spacecraft, one inertial and the other nadir pointing. These results are summarized in a later section.

State Vector Parameters

The state vector parameters $\boldsymbol{x}(t)$ are chosen to be identical to the nine elements of IRP as given in Ref. 5:

$$\boldsymbol{x}(t) \triangleq [\boldsymbol{\theta}(t) \quad \boldsymbol{\omega}(t) \quad \dot{\boldsymbol{\omega}}(t)]^T \tag{1}$$

$$\boldsymbol{\theta}(t) \triangleq [\theta_1(t) \quad \theta_2(t) \quad \theta_3(t)] \tag{2}$$

$$\boldsymbol{\omega}(t) \triangleq [\omega_1(t) \quad \omega_2(t) \quad \omega_3(t)] \tag{3}$$

$$\dot{\boldsymbol{\omega}}(t) \triangleq [\dot{\omega}_1(t) \quad \dot{\omega}_2(t) \quad \dot{\omega}_3(t)] \tag{4}$$

where $\boldsymbol{\theta}(t)$ is the vector of incremental angle (infinitesimal rotation vector), $\boldsymbol{\omega}(t)$ is the vector of angular velocity, and $\dot{\boldsymbol{\omega}}(t)$ is the vector of angular acceleration. All of the vectors are defined in the spacecraft body frame.

Measurement Model

At time t_k, any star vector estimated in the body frame is $\hat{\boldsymbol{v}}(k)$, and the same star tracked and measured at time t_{k+1} is $\boldsymbol{v}(k+1)$. Initially, in the absence of any better estimate, the available measurement $\boldsymbol{v}(k)$ at time t_k may be used to estimate the star vector $\hat{\boldsymbol{v}}(k)$, which will be refined later by using a recursive least-square estimate.

These vectors are related by the following expression when the rotation vector $\boldsymbol{\Delta\theta} \triangleq [\boldsymbol{\theta}(k+1) - \hat{\boldsymbol{\theta}}(k)]$ is infinitesimally small[17]:

$$\begin{bmatrix} v_1(k+1) \\ v_2(k+1) \\ v_3(k+1) \end{bmatrix} = \begin{bmatrix} 1 & \Delta\theta_3 & -\Delta\theta_2 \\ -\Delta\theta_3 & 1 & \Delta\theta_1 \\ \Delta\theta_2 & -\Delta\theta_1 & 1 \end{bmatrix} \begin{bmatrix} \hat{v}_1(k) \\ \hat{v}_2(k) \\ \hat{v}_3(k) \end{bmatrix} + \begin{bmatrix} n_1(k+1) \\ n_2(k+1) \\ n_3(k+1) \end{bmatrix} \tag{5}$$

where the last term $\boldsymbol{n}_a(k+1)$ in Eq. (5) represents the tracker measurement noise. After rearranging the terms,

$$\begin{bmatrix} v_1(k+1) - \hat{v}_1(k) \\ v_2(k+1) - \hat{v}_2(k) \\ v_3(k+1) - \hat{v}_3(k) \end{bmatrix} = \begin{bmatrix} 0 & -\hat{v}_3(k) & \hat{v}_2(k) \\ \hat{v}_3(k) & 0 & -\hat{v}_1(k) \\ -\hat{v}_2(k) & \hat{v}_1(k) & 0 \end{bmatrix} \begin{bmatrix} \Delta\theta_1 \\ \Delta\theta_2 \\ \Delta\theta_3 \end{bmatrix} + \boldsymbol{n}_a(k+1) \tag{6}$$

Equation (6) is of the form

$$\boldsymbol{z}_a(k+1) = \boldsymbol{H}_a(k+1)\Delta\theta + \boldsymbol{n}_a(k+1) \tag{7}$$

where

$$\boldsymbol{z}_a(k+1) \triangleq [\boldsymbol{v}(k+1) - \hat{\boldsymbol{v}}(k)] \tag{8}$$

Equation (7) can be rewritten as

$$\boldsymbol{z}_a(k+1) = \boldsymbol{H}_a(k+1)\boldsymbol{\theta}(k+1) + \boldsymbol{n}_a(k+1) \tag{9}$$

since

$$\boldsymbol{\Delta\theta} = [\boldsymbol{\theta}(k+1) - \hat{\boldsymbol{\theta}}(k)] \tag{10}$$

$$\hat{\boldsymbol{\theta}}(k) = 0 \tag{11}$$

due to full reset control.[5]

Please note that though the measurement model (9) is formulated as a linear equation, the sensitivity matrix $\boldsymbol{H}_a(k+1)$ depends on the $\hat{\boldsymbol{v}}(k)$. This implies that the Kalman filter gain cannot be computed a priori as might have been done on many suboptimal onboard filter implementations.

However, as observed in Ref. 8, the sensitivity matrix $\boldsymbol{H}_a(k+1)$ is a singular matrix because its determinant is zero. This implies that one of the rows is a linear combination of the other two rows and that no additional information is available in a single star measurement. Hence, to remedy this ill-conditioned problem, the row corresponding to the star tracker boresight axis measurement is left out because it is less sensitive. According to the star tracker axis definitions shown in Fig. 1, the boresight is located along the axis 1, and hence, the top row is deleted. This singularity implies that at least two star measurements, which are not collinear, are required for satisfactory estimation. The accuracy of the estimation improves if the measured stars are widely separated and will be highest if the measurements are made in orthogonal directions.[11]

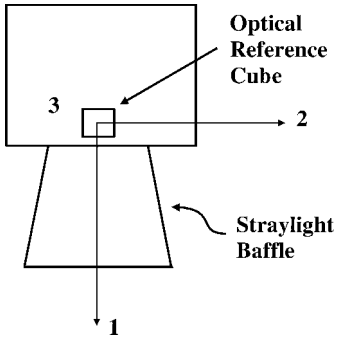

Fig. 1 Axis definitions of the star tracker.

The modified sensitivity matrix $\boldsymbol{H}_b(k+1)$, measurement $\boldsymbol{z}(k+1)$, and tracker noise $\boldsymbol{n}_b(k+1)$ are given as follows:

$$\boldsymbol{H}_b(k+1) = \begin{bmatrix} \hat{v}_3(k) & 0 & -\hat{v}_1(k) \\ -\hat{v}_2(k) & \hat{v}_1(k) & 0 \end{bmatrix} \tag{12}$$

$$\boldsymbol{z}(k+1) = \begin{bmatrix} v_2(k+1) - \hat{v}_2(k) \\ v_3(k+1) - \hat{v}_3(k) \end{bmatrix} \tag{13}$$

$$\boldsymbol{n}_b(k+1) = \begin{bmatrix} n_2(k+1) \\ n_3(k+1) \end{bmatrix} \tag{14}$$

The modified measurement model is given as

$$\boldsymbol{z}(k+1) = \boldsymbol{H}_b(k+1)\boldsymbol{\theta}(k+1) + \boldsymbol{n}_b(k+1) \tag{15}$$

When the sensitivity matrix is extended for the full state vector $\boldsymbol{x}(k+1)$ elements,

$$\boldsymbol{H}(k+1) = [\boldsymbol{H}_b(k+1)\,\boldsymbol{0}_{2\times 6}] \tag{16}$$

The full measurement model is given by

$$\boldsymbol{z}(k+1) = \boldsymbol{H}(k+1)\boldsymbol{x}(k+1) + \boldsymbol{n}_b(k+1) \tag{17}$$

Attitude Matrix

The attitude of the spacecraft is represented by an orthogonal direction cosine matrix (DCM) $\boldsymbol{D}(k)$ with respect to an arbitrary time t_0, which may be chosen as the start of the star tracker operation. If the absolute inertial-to-body attitude matrix $\boldsymbol{D}_{\mathrm{IB}}(0)$ of the spacecraft is known at this time instant, the DCM may be initialized as follows:

$$\boldsymbol{D}(0) = \boldsymbol{D}_{\mathrm{IB}}(0) \tag{18}$$

If the inertial attitude of the spacecraft is not known (lost-in-space condition), the DCM may be initialized with an identity matrix at time t_0 as follows:

$$\boldsymbol{D}(0) = \boldsymbol{I} \tag{19}$$

In this case, the absolute inertial attitude matrix can be computed later, after observation of sufficient number of stars for successful star pattern identification. The attitude matrix is defined such that its transpose will transform the star measurement vectors $\boldsymbol{v}(k)$ into the reference vectors $\boldsymbol{u}(0)$ that would have been observed at time t_0 in the body frame,

$$\boldsymbol{u}(0) = \boldsymbol{D}^T(k)\boldsymbol{v}(k) \tag{20}$$

The attitude matrix $\boldsymbol{D}(k+1)$ is propagated using the estimated state vector elements $\hat{\boldsymbol{x}}(k+1)$ on every time step and updated after every measurement update. This matrix is orthogonalized after the preceding steps. These operations are explained in the later sections.

Kalman Filter

The Kalman filter implementation consists of a time propagation of the state vector elements and a refinement based on the available actual star tracker measurement updates performed at discrete intervals of time steps.[18] These are summarized in the following sections.

Initialization

The filter state vector $\hat{\boldsymbol{x}}(k)$ and the error covariance matrix $\boldsymbol{P}(k)$ at time step $k = 0$ are initialized as follows:

$$\hat{\boldsymbol{x}}(0) = \boldsymbol{0} \tag{21}$$

$$\boldsymbol{P}(0) = \boldsymbol{0} \tag{22}$$

Time Propagation

The estimated filter state $\hat{\boldsymbol{x}}(k\,|\,k)$ and error covariance matrix $\boldsymbol{P}(k\,|\,k)$ at step t_k are propagated to $\hat{\boldsymbol{x}}(k+1\,|\,k)$ and $\boldsymbol{P}(k+1\,|\,k)$, respectively, at time t_{k+1} using the state transition matrix $\Phi(T)$, where $T \triangleq [t_{k+1} - t_k]$, as given in the following equations[5]:

$$\hat{\boldsymbol{x}}(k+1\,|\,k) = \Phi(T)\hat{\boldsymbol{x}}(k\,|\,k) \tag{23}$$

$$\boldsymbol{P}(k+1\,|\,k) = \Phi(T)\boldsymbol{P}(k\,|\,k)\Phi^T(T) + \boldsymbol{Q}(k) \tag{24}$$

$$\Phi(T) \triangleq \begin{bmatrix} \boldsymbol{I} & T\boldsymbol{I} & \Lambda^{-2}(e^{-\Lambda T} - \boldsymbol{I} + T\Lambda) \\ 0 & \boldsymbol{I} & \Lambda^{-1}(\boldsymbol{I} - e^{-\Lambda T}) \\ 0 & 0 & e^{-\Lambda T} \end{bmatrix} \tag{25}$$

The process noise covariance matrix $\boldsymbol{Q}(k)$ in Eq. (24) is a symmetric matrix whose upper diagonal elements are

$$Q_{11}(k) = \Lambda^{-4}\Sigma^2\big(\boldsymbol{I} + 2\Lambda T - 2\Lambda^2T^2 + \tfrac{2}{3}\Lambda^3T^3 - e^{-2\Lambda T} - 4\Lambda T e^{-\Lambda T}\big) \tag{26}$$

$$Q_{12}(k) = \Lambda^{-3}\Sigma^2(\boldsymbol{I} - 2\Lambda T + \Lambda^2T^2 - 2e^{-\Lambda T} + e^{-2\Lambda T} + 2\Lambda T e^{-\Lambda T}) \tag{27}$$

$$Q_{13}(k) = \Lambda^{-2}\Sigma^2(\boldsymbol{I} - e^{-2\Lambda T} - 2\Lambda T e^{-\Lambda T}) \tag{28}$$

$$Q_{22}(k) = \Lambda^{-2}\Sigma^2(4e^{-\Lambda T} - 3\boldsymbol{I} - e^{-2\Lambda T} + 2\Lambda T) \tag{29}$$

$$Q_{23}(k) = \Lambda^{-1}\Sigma^2(e^{-2\Lambda T} + \boldsymbol{I} - 2e^{-\Lambda T}) \tag{30}$$

$$Q_{33}(k) = \Sigma^2(\boldsymbol{I} - e^{-2\Lambda T}) \tag{31}$$

where

$$\Lambda \triangleq \text{diag}\{1/\tau_1, 1/\tau_2, 1/\tau_3\} \tag{32}$$

$$\Sigma \triangleq \text{diag}\{\sigma_1, \sigma_2, \sigma_3\} \tag{33}$$

Note that the constants $\tau_{1,2,3}$ in Eq. (32) are the acceleration decorrelation times along the corresponding spacecraft body axes and that the parameters $\sigma_{1,2,3}$ are the noise variances obtained by Singer acceleration probabilistic model[19] (also see Ref. 5). Fortunately, Eqs. (25–31) for $\Phi(T)$ and $\boldsymbol{Q}(k)$ can be computed a priori on the ground for each operation mode of the spacecraft and be uplinked to the onboard computer.

Measurement Update

When a star enters the FOV, the tracker detects the star presence, forms a track window around the star image, and allocates a unique track number. All of the subsequent measurements of that star are tagged with the same track number. If the star leaves the FOV and reenters again or if the tracking is broken due to any reason, another new track number may be given by the star tracker software. However, with the help of the track numbers, it is possible to correlate the temporal measurements of the stars being tracked. Alternatively, consistency in the visual magnitude or angular separation of the star patterns between the previous and present observation frames can also be made use of.

The tracker outputs the direction cosines (DCs) of the star tracked $\boldsymbol{v}_s(k+1)$ in the tracker coordinate frame. These DCs are transformed into the spacecraft body reference frame $\boldsymbol{v}_b(k+1)$ using the sensor-to-body alignment matrix $\boldsymbol{D}_{\text{SB}}$ as follows:

$$\boldsymbol{v}_b(k+1) = \boldsymbol{D}_{\text{SB}}\boldsymbol{v}_s(k+1) \tag{34}$$

When n stars are being tracked in the FOV of the tracker, the DCs of the ith star-look vector in the body frame $\boldsymbol{v}_i(k+1)$ are measured at time step t_{k+1} and the same star's best known DCs in the body frame in the previous time instant t_k are $\hat{\boldsymbol{v}}_i(k)$. The difference in DCs $\boldsymbol{z}_i(k+1)$ is computed as

$$\boldsymbol{z}_i(k+1) = \begin{bmatrix} v_{i2}(k+1) - \hat{v}_{i2}(k) \\ v_{i3}(k+1) - \hat{v}_{i3}(k) \end{bmatrix} \tag{35}$$

The modified measurement sensitivity matrix $\boldsymbol{H}_i(k+1)$ is given by Eqs. (12) and (16) applied for each star vector. The equations governing measurement update to the state vector are given as follows:

$$\boldsymbol{y}_i(k+1) = \boldsymbol{z}_i(k+1) - \boldsymbol{H}_i(k+1)\,\hat{\boldsymbol{x}}(k+1\,|\,k) + \boldsymbol{n}(k+1) \tag{36}$$

The measurement noise $\boldsymbol{n}(k+1)$ in Eq. (36) is assumed to be white noise with Gaussian characteristics $\mathcal{N}[0, \boldsymbol{R}(k+1)]$, where

$$\boldsymbol{R}(k+1) = \begin{bmatrix} R'_{22}(k+1) & R'_{23}(k+1) \\ R'_{32}(k+1) & R'_{33}(k+1) \end{bmatrix} \tag{37}$$

The covariance matrix $\boldsymbol{R}$ is of dimension 2×2 corresponding to only the sensitive measurement axes of the star tracker and is obtained by deleting the first row and first column corresponding to the boresight axis of the tracker from the matrix $\boldsymbol{R}'$,

$$\boldsymbol{R}'(k+1) \triangleq \boldsymbol{R}_v(k+1) + \hat{\boldsymbol{D}}(k+1\,|\,k)\boldsymbol{R}_u(k+1)\hat{\boldsymbol{D}}^T(k+1\,|\,k) \tag{38}$$

where $\boldsymbol{R}_v(k+1)$ is the tracker measurement noise covariance matrix, $\boldsymbol{R}_u(k+1)$ is the error covariance matrix of the estimated DCs of the reference star in the body frame, and $\hat{\boldsymbol{D}}(k+1\,|\,k)$ is the latest direction cosine matrix, which projects the reference uncertainty to the measurement plane. All of these matrices are of 3×3 dimension.

The Kalman filter gain matrix is computed by

$$\boldsymbol{K}'(k+1) \triangleq \boldsymbol{P}(k+1\,|\,k)\boldsymbol{H}_i^T(k+1) \tag{39}$$

$$\boldsymbol{K}(k+1) = \boldsymbol{K}'(k+1) \times [\boldsymbol{H}_i(k+1)\boldsymbol{K}'(k+1) + \boldsymbol{R}(k+1)]^{-1} \tag{40}$$

Note that the inverse in the preceding equation needs to be computed only for a 2×2 matrix. The state measurement update equation is

$$\hat{\boldsymbol{x}}(k+1\,|\,k+1) = \hat{\boldsymbol{x}}(k+1\,|\,k) + \boldsymbol{K}(k+1)\boldsymbol{y}_i(k+1) \tag{41}$$

The error covariance matrix is updated using Joseph's propagation algorithm, which is numerically superior to the standard form (see Ref. 18, page 305) as follows:

$$\boldsymbol{S}(k+1) \triangleq [\boldsymbol{I} - \boldsymbol{K}(k+1)\boldsymbol{H}_i(k+1)] \tag{42}$$

$$\boldsymbol{P}(k+1\,|\,k+1) = [\boldsymbol{S}(k+1)\boldsymbol{P}(k+1\,|\,k)\boldsymbol{S}^T(k+1) + \boldsymbol{K}(k+1)\boldsymbol{R}(k+1)\boldsymbol{K}^T(k+1)] \tag{43}$$

Note that Eqs. (35–43) are computed iteratively for all of the stars tracked, $i = 1, 2, \ldots, n$, using the latest state vector $\hat{\boldsymbol{x}}(k+1)$ and state covariance matrix $\boldsymbol{P}(k+1)$.

DCM Update

After all of the measurements are processed, the current orthogonalized estimate of the DCM $\hat{\boldsymbol{D}}^*(k\,|\,k)$ at time t_k is updated to t_{k+1} using the latest updated state vector elements $\hat{\boldsymbol{x}}(k+1)$. This is done as follows[5]:

$$\hat{\boldsymbol{D}}(k+1\,|\,k+1) = \big[\boldsymbol{I} + \hat{\boldsymbol{A}}(k+1) + \tfrac{1}{2}\hat{\boldsymbol{A}}^2(k+1) + \tfrac{1}{6}\hat{\boldsymbol{A}}^3(k+1) + \hat{\boldsymbol{C}}(k+1)\big]\hat{\boldsymbol{D}}^*(k\,|\,k) \tag{44}$$

where

$$\hat{\boldsymbol{C}}(k+1) = \tfrac{1}{6}T[\hat{\boldsymbol{A}}(k+1)\hat{\boldsymbol{\Psi}}(k+1\,|\,k+1) - \hat{\boldsymbol{\Psi}}(k+1\,|\,k+1)\hat{\boldsymbol{A}}(k+1)] \tag{45}$$

$$\hat{\boldsymbol{A}}(k+1) \triangleq -[\hat{\boldsymbol{\theta}}(k+1\,|\,k+1)\otimes] \tag{46}$$

$$\hat{\boldsymbol{\Psi}}(k+1\,|\,k+1) \triangleq -[\hat{\psi}(k+1\,|\,k+1)\otimes] \tag{47}$$

$$\hat{\psi}(k+1\,|\,k+1) \triangleq [\hat{\boldsymbol{\omega}}(k+1\,|\,k+1) - T\hat{\dot{\boldsymbol{\omega}}}(k+1\,|\,k+1)] \tag{48}$$

$$\hat{\boldsymbol{\theta}}(k+1\,|\,k+1) \equiv \hat{\boldsymbol{x}}_j(k+1\,|\,k+1), \qquad j = 1, 2, 3 \tag{49}$$

$$\hat{\omega}(k+1\,|\,k+1) \equiv \hat{x}_j(k+1\,|\,k+1), \qquad j=4,5,6 \tag{50}$$

$$\hat{\dot{\omega}}(k+1\,|\,k+1) \equiv \hat{x}_j(k+1\,|\,k+1), \qquad j=7,8,9 \tag{51}$$

$$T \triangleq t_{k+1} - t_k \tag{52}$$

Here, $[\boldsymbol{a}\otimes]$ denotes the skew symmetric cross-product matrix formed by the given vector $\boldsymbol{a}$:

$$[\boldsymbol{a}\otimes] \triangleq \begin{bmatrix} 0 & -a_3 & a_2 \\ a_3 & 0 & -a_1 \\ -a_2 & a_1 & 0 \end{bmatrix} \tag{53}$$

DCM Orthogonalization

To maintain the properties of the DCM[17] after the time-propagation step and even after the measurement update, a single-step iterative orthogonalization procedure is performed.[20,21] These steps are outlined as follows:

$$\boldsymbol{N}(k+1) = \left[\tfrac{3}{2}\boldsymbol{I} - \tfrac{1}{2}\hat{\boldsymbol{D}}(k+1\,|\,k+1)\hat{\boldsymbol{D}}^T(k+1\,|\,k+1)\right] \tag{54}$$

$$\hat{\boldsymbol{D}}^*(k+1\,|\,k+1) = \boldsymbol{N}(k+1)\hat{\boldsymbol{D}}(k+1\,|\,k+1) \tag{55}$$

Reset Control

After each step of propagation of the state vector $\hat{\boldsymbol{x}}(k+1\,|\,k)$ and update with the measurement $\hat{\boldsymbol{x}}(k+1\,|\,k+1)$, the first three elements of the estimated state vector, which are used for the next step, are reset to zero. This is because the effect of the spacecraft motion for this interval is already included in the DCM $[\hat{\boldsymbol{D}}^*(k+1\,|\,k+1)]$ from the propagated state vector elements, and the incremental angle $\boldsymbol{\theta}$ may be fully reset to zero at the beginning of the next interval,

$$\hat{x}_j(k) = 0, \qquad j=1,2,3 \tag{56}$$

Star Map on Body Frame

All of the star vectors $\boldsymbol{v}_i(k+1)$ measured at time step t_{k+1} are mapped on to the body frame using the inverse of the attitude matrix (the transpose of the DCM) with epoch at time step t_0, which is an arbitrary time of start of star tracker operation. This will serve as the reference catalog for future star measurements,

$$\boldsymbol{u}_i(k+1) = \hat{\boldsymbol{D}}^{*T}(k+1\,|\,k+1)\boldsymbol{v}_i(k+1), \qquad i=1,2,\ldots,n \tag{57}$$

The star vectors thus collapsed onto the body frame are refined using successive measurements and a recursive unbiased minimum variance estimate (recursive average estimate).[18] This is computed as follows:

$$\hat{\boldsymbol{u}}_i(k+1) = \hat{\boldsymbol{u}}_i(k) + [1/(k+1)][\boldsymbol{u}_i(k+1) - \hat{\boldsymbol{u}}_i(k)] \qquad i=1,2,\ldots,n \tag{58}$$

$$\hat{\boldsymbol{u}}_i(0) = \boldsymbol{0} \tag{59}$$

After computing the best estimate of the star vectors in the body frame referred to an arbitrary epoch, these vectors are normalized to preserve the unit vector norm:

$$\hat{\boldsymbol{u}}_i^*(k+1) = \frac{\hat{\boldsymbol{u}}_i(k+1)}{\|\hat{\boldsymbol{u}}_i(k+1)\|}, \qquad i=1,2,\ldots,n \tag{60}$$

These estimates of ideal star positions from the body frame with epoch t_0 is further transformed to time step t_{k+1} using the orthogonalized recent DCM $\hat{\boldsymbol{D}}^*(k+1\,|\,k+1)$ to satisfy the assumption that the incremental angle is infinitesimally small,

$$\hat{\boldsymbol{v}}_i(k+1) = \hat{\boldsymbol{D}}^*(k+1\,|\,k+1)\hat{\boldsymbol{u}}_i^*(k+1), \qquad i=1,2,\ldots,n \tag{61}$$

Thus, the best estimates of the star vectors $\hat{\boldsymbol{v}}_i(k+1)$ as computed from Eq. (61) are used to compute the vector difference in Eq. (35) at the next time step.

Star Identification

The absolute inertial attitude matrix of the spacecraft $\hat{\boldsymbol{D}}_{\mathrm{IB}}(k+1)$ can be computed once the orientation of the regenerated star map on the unit body sphere $\hat{\boldsymbol{D}}_{\mathrm{IB}}(0)$ is known with respect to the inertial sphere in the lost-in-space condition.

$$\hat{\boldsymbol{D}}_{\mathrm{IB}}(k+1) = \hat{\boldsymbol{D}}^*(k+1)\,\hat{\boldsymbol{D}}_{\mathrm{IB}}(0) \tag{62}$$

The matrix $\hat{\boldsymbol{D}}_{\mathrm{IB}}(0)$ in Eq. (62) can be computed[22] by matching the star patterns on the map to that of the reference star catalog by any star pair identification technique.[16] Many star identification algorithms assume that the angular separation between the observed stars is limited by the FOV of the star tracker, and this assumption is generally not valid for the star map generated using the present method.

Note that the effects of the measurement noise are minimized because the star map is generated by averaging many observations. If the spacecraft has considerable body rates, the probability of observing the bright stars increases. A small catalog will be sufficient to use for bright stars. Star identification can be carried out even from the combined observations of multiple star trackers using the associated star maps generated on the body frame. These factors help in reliable star identification with a minimum computational overhead.

Numerical Simulation

To illustrate the described method, two numerical simulations are performed. The first problem is identical to that given in Ref. 5, that is, an inertial pointing spacecraft with initial attitude errors of $\phi_1 = 10$, $\phi_2 = 20$, and $\phi_3 = 30$ deg, where ϕ_i is the Euler angle rotation about a body axis i defined in a 3–2–1 rotation sequence. The true angular rate (degrees per second) of the body is time varying as

$$\omega(t) = \begin{bmatrix} 0.02\sin[(2\pi/85)t + (\pi/4)] \\ 0.05\sin[(2\pi/45)t + (\pi/2)] \\ 0.03\sin[(2\pi/65)t + (3\pi/4)] \end{bmatrix} \tag{63}$$

In solving this problem, Oshman and Markley have generated the reference vectors randomly at each measurement epoch.[5] We notice that this procedure does not represent a typical onboard situation because any practical sensor has only a limited FOV. The procedure in Ref. 5 amounts to having infinite number of sensors on the spacecraft, giving out the measurements in all directions, which is impractical. To assess the performance in a real world situation, a single star tracker with a 20×20 deg FOV is used in this simulation study with the definitions of axis 1 aligned with the boresight and the remaining two axes perpendicular to the boresight axis in a right-handed system (Fig. 1). To simplify the scenario, the star tracker is assumed to be mounted along the axis 1 of the spacecraft. (The sensor-to-body mounting matrix $\boldsymbol{D}_{\mathrm{SB}}$ is unity.) The measurement noise of the star tracker[23] is assumed to be 5 arc-s (1σ) in the measurement plane (axes 2 and 3) and 20 arc-s (1σ) around the boresight axis 1.

To study the effect of star availability on the algorithms, a subcatalog of 1638 stars up to 5.0 visual magnitude is drawn from the SKYMAP 2000 star catalog. The spacecraft motion is integrated using Simpson's one-third rule with given body rates transformed into Euler rotation axes (see Ref. 24), and the attitude DCM is computed. By the use of this DCM, the coordinates of the stars seen by the star tracker at a given time instant are computed from the star subcatalog.

Figure 2 shows the FOV of the star tracker on the celestial sphere. Figure 3 shows the FOV more closely. A total of five stars can be seen in the FOV. The black blob in the center is the trace of the boresight of the star tracker indicating the integrated effect of motion. The measurements are corrupted by the Gaussian noise corresponding to the tracker measurement noise, and the catalog positions of the stars are corrupted by a reference uncertainty 5 arc-s ($1\,\sigma$). The rest of the constants (such as parameters of the spacecraft motion model, etc.) used in the problem simulation are identical to the ones given in Ref. 5.

First, the spacecraft attitude and angular rate are computed for 200 s using the method given in Ref. 5. Note that all of the star

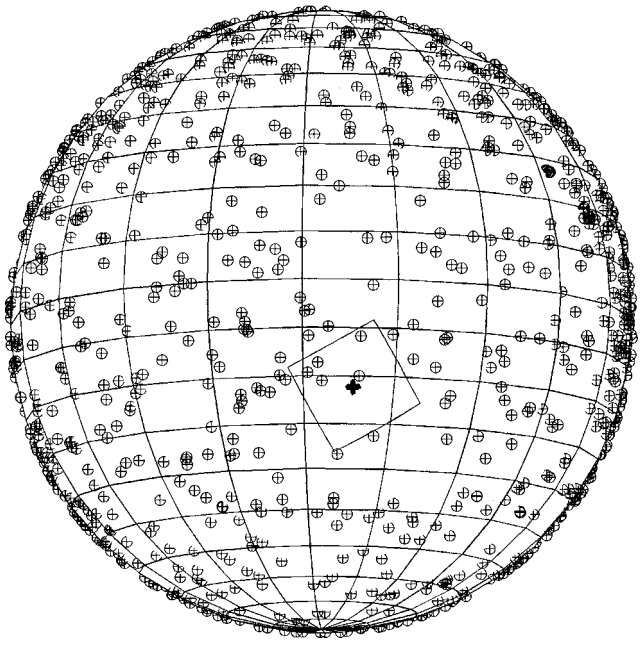

Fig. 2 Star tracker FOV on the celestial sphere.

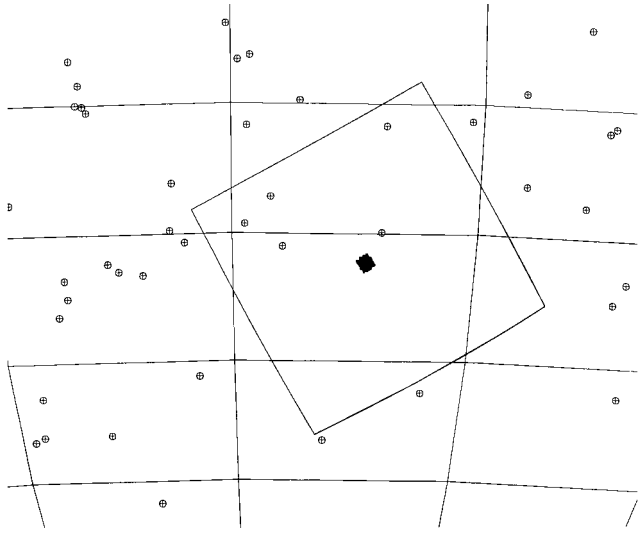

Fig. 3 Closeup of the FOV of the star tracker.

measurement vectors in the FOV along with their corresponding star catalog reference vectors are used in the measurement update equations (46), (48), and (57) given in Ref. 5. Here the measurements are sampled at 10 Hz, whereas the propagation of filter state and error covariance is carried out at 20 Hz. Later, the same star measurement vectors are processed using the new SIAVE method already described, without using the reference vectors from the star catalog. These results are given in the next section.

In the second problem, an identical star tracker is assumed to be mounted on the nadir pointing spacecraft such as the Indian Remote Sensing (1D) spacecraft. The star tracker boresight is along the negative yaw axis (axis 1) of the spacecraft, that is, always pointing away from the Earth. This is achieved by initially aligning the star tracker axes with those of the spacecraft and then giving a 180-deg rotation about the axis 3 (pitch axis). This causes the FOV to scan the celestial sphere in a 20-deg-wide belt with the spacecraft motion. The stars enter the FOV and leave after a fixed duration. The position (kilometers) and velocity vectors (kilometers per second) of the spacecraft at the start of the simulation are given in the Earth centered inertial frame as follows:

$$\text{position} = \begin{bmatrix} -4413.868568 \\ -1706.875721 \\ 5424.426007 \end{bmatrix} \tag{64}$$

$$\text{velocity} = \begin{bmatrix} -5.686326 \\ -0.383843 \\ -4.750019 \end{bmatrix} \tag{65}$$

In this case, to illustrate the performance of the filter, no attitude errors other than the orbital rate introduced by nadir pointing are simulated. Again, the SIAVE filter is run with a 20-Hz update frequency for state and covariance propagation, and star measurements are made at a 10-Hz frequency. The results are analyzed in the next section.

Results

For the first problem simulated, that is, the inertial pointing spacecraft attitude estimation, Figs. 4–6 show the comparison of residuals (estimated–simulated) of the angular rate estimation about all of the three spacecraft axes. Figures 4a–6a show the simulated angular rate about a given axis, Figs. 4b–6b show the angular rate errors estimated by Oshman and Markley's method[5] and Figs. 4c–6c show the angular rate errors estimated by using the SIAVE method. The two horizontal lines in Figs. 4b–6b and Figs. 4c–6c indicate the upper and lower 3σ limits of the estimation error (three times the square root of the corresponding diagonal covariance term) for each axis.

For the angular rate estimation carried out using the method of Oshman and Markley,[5] it can be clearly seen from Fig. 4b that the rate estimation is relatively poor around axis 1 of the spacecraft compared to the other two axes. This is due to the insensitivity of the star tracker around that axis due to the mounting. Rate estimation around the other two axes is satisfactory in Figs. 5b and 6b. The initial transient is large in all of the three axes as seen in Figs. 4b–6b. It can be seen that the EKF suggested by Ref. 5 is hunting for the proper solution because the linearized measurement equations will hold a proper gradient only for a very narrow range of values. As a result, the estimation does not converge for 20 s from the start of simulation. On the positive side, it can be seen that the rate estimation residuals are small, limited only by the star tracker measurement noise, even when the angular rate vector

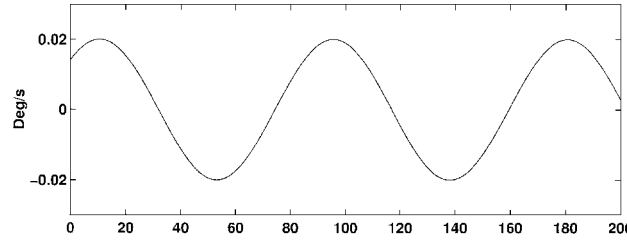

a) Simulated spacecraft angular rate about axis 1

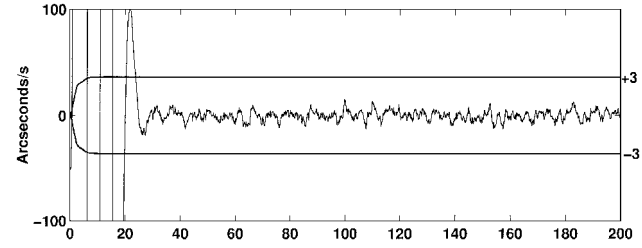

b) Estimated angular rate error with Oshman and Markley's method[5]

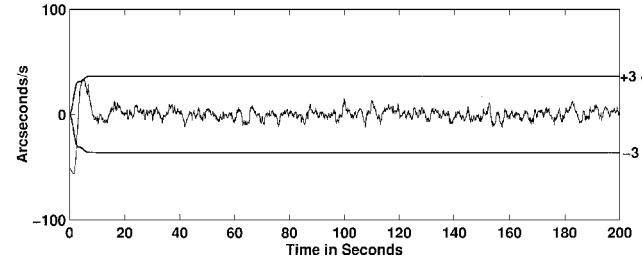

c) Estimated angular rate error with SIAVE method

Fig. 4 Comparison of angular rate estimation about axis 1.

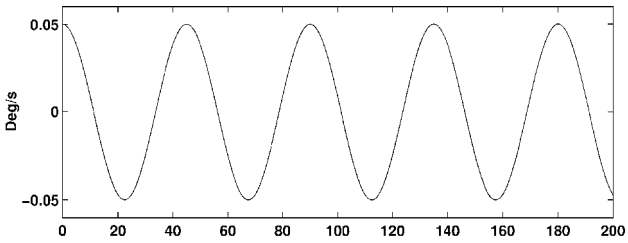

a) Simulated spacecraft angular rate about axis 2

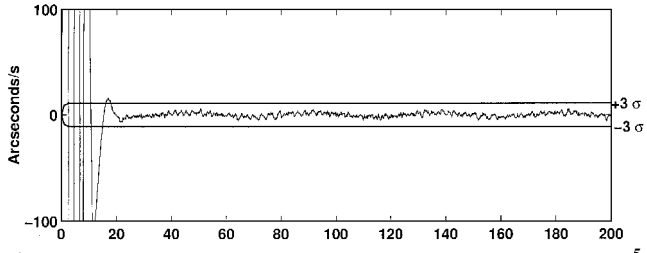

b) Estimated angular rate error with Oshman and Markley's method[5]

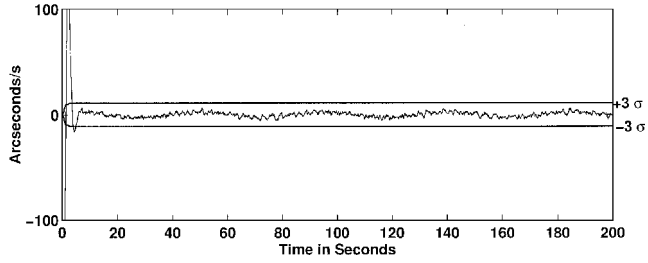

c) Estimated angular rate error with SIAVE method

Fig. 5 Comparison of angular rate estimation about axis 2.

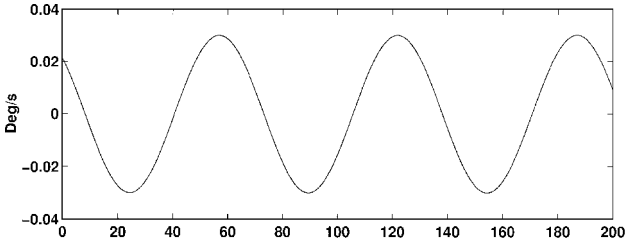

a) Simulated spacecraft angular rate about axis 3

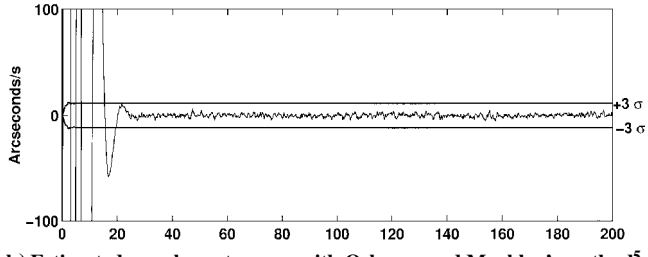

b) Estimated angular rate error with Oshman and Markley's method[5]

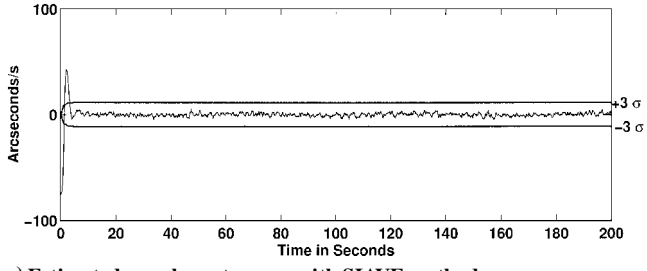

c) Estimated angular rate error with SIAVE method

Fig. 6 Comparison of angular rate estimation about axis 3.

is time varying. The higher-order kinematic modeling used by the IRP method does a good job, tracking the spacecraft attitude even with a single star tracker giving the measurements.

It can be seen from Figs. 4c–6c that the angular rate estimation carried out by the proposed SIAVE method in the inertial pointing case is as good as Oshman and Markley's method.[5] The higher rate noise seen in Fig. 4c is again due to the insensitivity of the star tracker to rotation around that axis (boresight). This noise is present in both methods (Figs. 4b and 4c) and is independent of the method. Table 1 gives the steady-state rate estimation error (3σ) limits in both the methods. It can be seen that the proposed SIAVE method is equally accurate compared to the earlier method.

Notice that the SIAVE method shows a quick convergence of the estimator for all of the three axes within 10 s from the beginning of the simulation run. This is the distinct advantage of the linear Kalman filter with linear equations of measurement compared to the EKF with nonlinear measurement equations. Thus, the proposed SIAVE filter will do better with a faster convergence, when a step input is encountered, compared to Oshman and Markley's method.[5] Also, the effect of uncertainty (noise) in the star reference positions (star catalog) will decrease with time, unlike Oshman and Markley's method, where it remains steady with time because there is no way of updating the star catalog from the measurements.

For the second problem simulated, the movement of the star tracker FOV in the celestial sphere due to spacecraft nadir pointing is shown in the Fig. 7. The center of the FOV is indicated by a + sign, which forms a thick slanted line during the simulation. The angular rate estimation carried out by the SIAVE filter for all of the axes is shown in Fig. 8. The 3σ limits of the rate estimation error are plotted as horizontal lines in Figs. 8a–8c. The steady-state rate estimation error 3σ limits for this case are given in the Table 1.

In Fig. 8a, corresponding to axis 1, a higher noise is seen in the estimated angular rate due to the poor sensitivity of the star tracker around the boresight axis. The estimation error 3σ limits also show a larger variation in the plot depending on the stars present in the FOV, but these are well within the bounds. The rate estimation about

Table 1 Steady-state rate estimation error (3σ) limits in arcsecond per second

Error	Ref. 5 method	SIAVE method
Inertial pointing		
ω_1	36.20	36.20
ω_2	11.02	11.03
ω_3	11.45	11.45
Nadir pointing		
ω_1		28.44
ω_2		9.47
ω_3		9.46

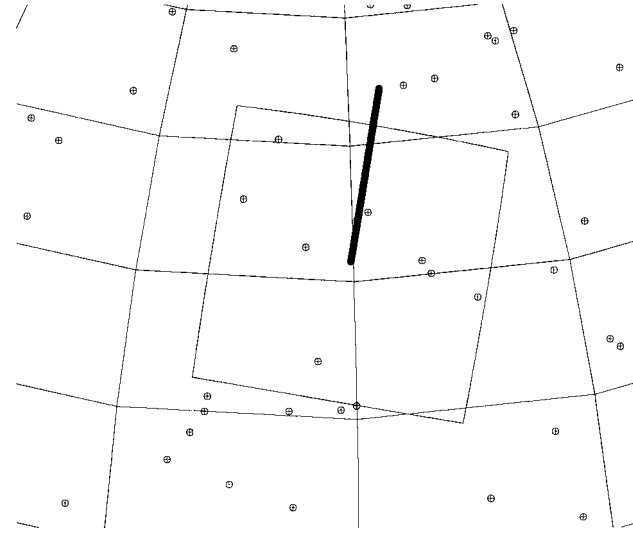

Fig. 7 FOV of the star tracker during the nadir pointing.

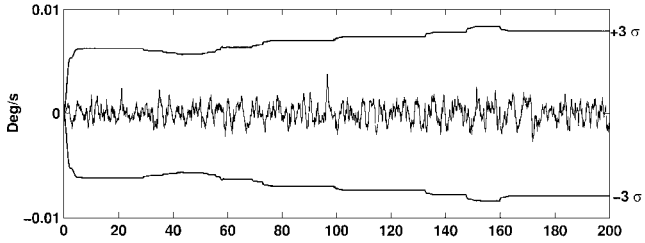

a) About axis 1

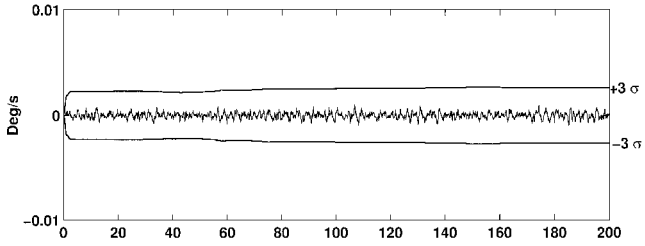

b) About axis 2

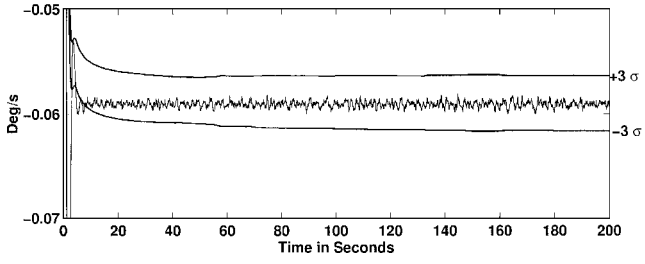

c) About axis 3

Fig. 8 Estimated angular rates for the nadir pointing using SIAVE method.

the other two axes is satisfactory. Note that the SIAVE filter is able to estimate the mean angular rate bias of −0.059 deg/s about axis 3 (pitch axis) due to nadir pointing accurately.

Figure 9 shows the reconstructed star map from the SIAVE filter. Figure 9 shows that the star measurements at different instants are combined to form a star map on a sphere. The labels on the map correspond to the subcatalog numbers of the stars simulated.

The angular separation is computed using the dot product of the star pairs simulated in the catalog and the dot product of the corresponding star pairs in the generated star map. Table 2 gives the difference in angular distances of the stars simulated and star map reconstructed in the body frame using the SIAVE method for the nadir pointing case. Note that the stars corresponding to an angular separation less than 1 deg are excluded from Table 2, while keeping all of the stars encountered even during the transient conditions of the filter. This shows that the angular distance between the stars is preserved to a high accuracy (3 arc-s 3σ). This proves that the incremental angle estimation and the attitude reconstruction using the SIAVE method are satisfactory.

To illustrate the method, a single star tracker with a 20×20 deg FOV is used, though this is not the ultimate. Present day star trackers[23] do better than the noise specifications assumed in this study. To improve the accuracies achievable in a nadir pointing spacecraft even further, the FOV of the star tracker may be reduced to 4×4 deg with two star trackers mounted on the spacecraft in two orthogonal directions.[11] This will improve the estimation of both angle and rate because the measurement noise of the star trackers will reduce to less than 1 arc-s (1σ) and insensitivity around the boresight axis of the first star tracker will be compensated for by the other star tracker.

In the initial attitude acquisition phase, the spacecraft can be put into rate control mode (spun around any spacecraft axis) using the rate obtained by the SIAVE filter using the star trackers alone, without a gyroscope. The spacecraft motion is integrated for a few seconds using the SIAVE filter, and the star map is generated. The star identification can be carried out with any of the traditional star pair identification techniques using only the bright stars of the star map. This will reduce the onboard star catalog memory requirements

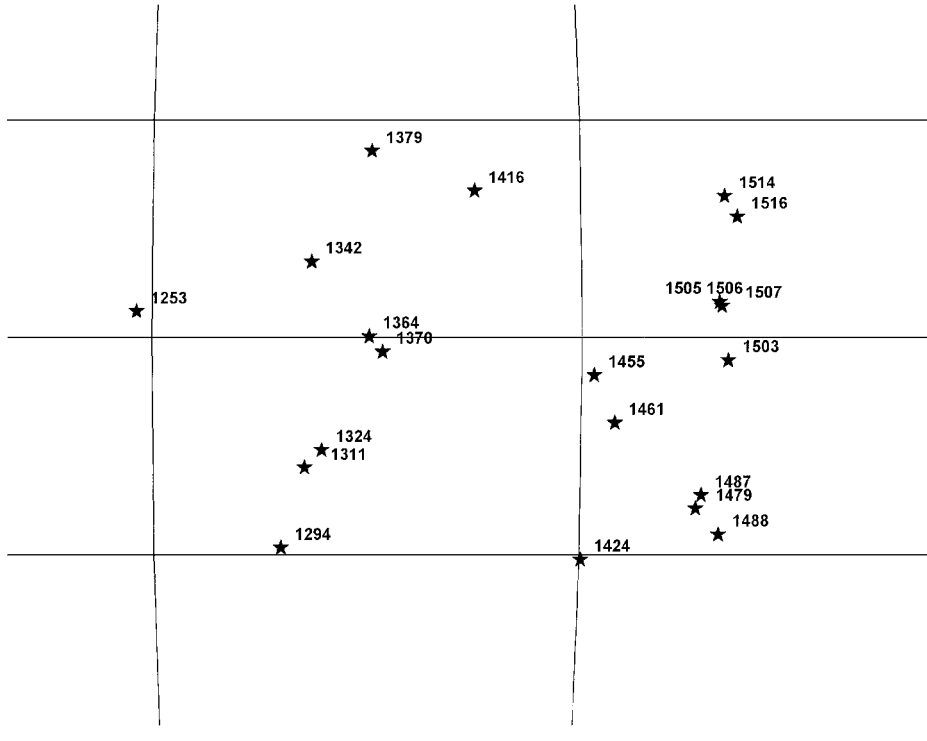

Fig. 9 Reconstructed star map using SIAVE method for the nadir pointing case.

Table 2 Angular separations of the star pairs

Star 1 number	Star 2 number	Catalog separation, deg	Map separation, deg	Difference, arc-s
1364	1379	7.661	7.661	0.1
1364	1416	7.441	7.441	0.7
1364	1424	12.853	12.853	−0.0
1370	1379	8.300	8.300	−0.3
1370	1416	7.662	7.662	0.2
1370	1424	12.012	12.012	−0.2
1379	1416	4.577	4.576	1.2
1379	1424	19.047	19.047	−0.1
1379	1455	13.117	13.117	−0.3
1416	1424	15.873	15.873	0.2
1416	1455	9.092	9.092	0.1
1416	1461	11.228	11.228	0.2
1424	1455	7.648	7.648	−0.5
1424	1461	5.823	5.823	−0.8
1424	1479	5.279	5.279	−0.7
1455	1461	2.159	2.160	−2.5
1455	1479	7.070	7.070	−0.6
1455	1487	6.802	6.803	−0.7
1461	1479	5.005	5.005	−1.0
1461	1487	4.805	4.805	−0.9
1461	1488	6.487	6.488	−1.2
1479	1503	6.267	6.267	−0.2
1479	1505	8.583	8.583	−0.8
1479	1506	8.586	8.586	0.3
1487	1503	5.684	5.684	−0.1
1487	1505	8.014	8.014	−0.9
1487	1506	8.017	8.017	0.3
1488	1503	7.215	7.215	−0.7
1488	1505	9.612	9.613	−1.3
1488	1506	9.616	9.616	−0.2
1505	1514	4.364	4.365	−1.3
1505	1516	3.577	3.578	−2.2
1505	1324	17.836	17.836	−0.6
1506	1514	4.362	4.362	0.6
1506	1516	3.574	3.574	0.3
1506	1324	17.840	17.840	−0.2
1507	1311	18.811	18.810	0.3
1507	1294	21.056	21.056	−0.0
1507	1253	24.608	24.608	−0.1
1516	1311	21.006	21.006	0.1
1516	1294	23.594	23.594	−0.1
1516	1253	25.581	25.581	−0.2

while eliminating the false star identifications and reducing the identification time.

Conclusions

A simple linear Kalman filter is proposed for estimation of incremental angle and angular rate from successive observations of a star tracker, without the use of star catalog or auxiliary sensors. This incremental angle and angular rate output can be directly used in the spacecraft control system because the output is similar to that of a rate integrating gyroscope. The star map built by using this method can be used for the purpose of star pair identification, which will reduce the onboard memory requirements and eliminate the false star identifications. The accuracy obtained using this method is demonstrated by numerical simulations carried out for the inertial pointing case and compared with that of Oshman and Markley's method.[5] The filter performance is satisfactory, with the additional advantage of a faster convergence. In another numerical simulation of an Earth pointing spacecraft, the angular separations between the simulated star catalog and that obtained from the regenerated star map match very closely, proving the estimation of incremental angle. Finally, a method to improve the attitude and rate estimation accuracy is outlined for Earth pointing spacecraft.

Acknowledgments

The authors wish to thank P. S. Goel, Director, Indian Space Research Organization (ISRO) Satellite Center and Kasturi Rangan, Chairman, ISRO for their encouragement in carrying out research in the exciting field of star sensor attitude determination. The first author wishes to acknowledge the support received by him in carrying out this work and for many important suggestions from J. Srinivasa Rao, T. H. Shashikala, and the other colleagues. Finally, the authors are grateful to the anonymous reviewers and the editorial staff of this journal for their constructive suggestions in improving the technical content as well as the presentation of this paper.

References

[1]Liebe, C. C., "Star Trackers for Attitude Determination," *IEEE Aerospace and Electronic Systems Magazine*, Vol. 10, No. 6, 1995, pp. 10–16.

[2]Liebe, C. C., "Pattern Recognition of Star Constellations for Spacecraft Applications," *IEEE Aerospace and Electronic Systems Magazine*, Vol. 8, No. 1, 1993, pp. 31–39.

[3]Shuster, M. D., and Oh, S. D., "Three Axis Attitude Determination from Vector Observations," *Journal of Guidance, Control, and Dynamics*, Vol. 4, No. 1, 1981, pp. 70–77.

[4]Markley, F. L., et al., "Attitude Control System Conceptual Design for Geostationary Operational Environmental Satellite Spacecraft Series," *Journal of Guidance, Control, and Dynamics*, Vol. 18, No. 2, 1995, pp. 247–255.

[5]Oshman, Y., and Markley, F. L., "Sequential Attitude and Attitude-Rate Estimation Using Integrated-Rate Parameters," *Journal of Guidance, Control, and Dynamics*, Vol. 22, No. 3, 1999, pp. 385–394.

[6]Challa, M., and Wheeler, C., "Accuracy Studies of a Magneto-Meter-Only Attitude-and-Rate-Determination System," *NASA Flight Mechanics Estimation Theory Symposium*, NASA-CP-3333, 1996, pp. 179–189.

[7]Gai, E., Daly, K., Harrison, J., and Lemos, L., "Star-Sensor Based Satellite Attitude/Attitude Rate Estimator," *Journal of Guidance, Control, and Dynamics*, Vol. 8, No. 5, 1985, pp. 560–565.

[8]Azor, R., Bar-Itzhack, I. Y., and Harman, R. R., "Satellite Angular Rate Estimation from Vector Measurements," *Journal of Guidance, Control, and Dynamics*, Vol. 21, No. 3, 1998, pp. 450–457.

[9]Harman, R. R., and Bar-Itzhack, I. Y., "Pseudolinear and State-Dependent Riccati Equation Filters for Angular Rate Estimation," *Journal of Guidance, Control, and Dynamics*, Vol. 22, No. 5, 1999, pp. 723–725.

[10]Bezooijen, R. W. H., "Autonomous Star Referenced Attitude Determination," *Advances in the Astronautical Sciences*, Vol. 68, 1989, pp. 31–52; also American Astronautical Society, Paper AAS 89-003, 1989.

[11]Mortari, D., Polloc, T. C., and Junkins, J. L., "Toward the Most Accurate Attitude Determinations System Using Star Trackers," *Advances in the Astronautical Sciences*, Vol. 99, Pt. 2, 1998, pp. 839–850; also American Astronautical Society, Paper AAS 98-159, 1998.

[12]Ketchum, E. A., and Tolson, R. H., "Onboard Star Identification Without a Priori Attitude Information," *Journal of Guidance, Control, and Dynamics*, Vol. 18, No. 2, 1995, pp. 242–246.

[13]Clouse, D. S., and Padgett, C. W., "Small Field-of-View Star Identification Using Bayesian Decision Theory," *IEEE Transactions on Aerospace and Electronic Systems*, Vol. 36, No. 3, 2000, pp. 773–783.

[14]Blanton, J. N., "Star Identification for Sensors with Nonsimultaneous Acquisition Times," *Journal of the Astronautical Sciences*, Vol. 30, No. 3, 1982, pp. 277–285.

[15]Udomkesmalee, S., Alexander, J. W., and Toliver, A. F., "Stochastic Star Identification," *Journal of Guidance, Control, and Dynamics*, Vol. 17, No. 6, 1994, pp. 1283–1286.

[16]Padgett, C., Kreutz-Delgado, K., and Udomkesmalee, S., "Evaluation of Star Identification Techniques," *Journal of Guidance, Control, and Dynamics*, Vol. 20, No. 2, 1997, pp. 259–267.

[17]Shuster, M. D., "A Survey of Attitude Representations," *Journal of the Astronautical Sciences*, Vol. 41, No. 4, 1993, pp. 445–453.

[18]Gelb, A., *Applied Optimal Estimation*, 1974 ed., MIT Press, Cambridge, MA, reprint 1988, pp. 105–119.

[19]Singer, R. A., "Estimating Optimal Tracking Filter Performance for Manned Maneuvering Targets," *IEEE Transactions on Aerospace and Electronic Systems*, Vol. AES-6, No. 4, 1970, pp. 473–483.

[20]Bar-Itzhack, I. Y., and Meyer, J., "On the Convergence of Iterative Orthogonalization Processes," *IEEE Transactions on Aerospace and Electronic Systems*, Vol. AES-12, No. 2, 1976, pp. 146–151.

[21]Björck, A., and Bowie, C., "An Iterative Algorithm for Computing the Best Estimate of an Orthogonal Matrix," *SIAM Journal on Numerical Analysis*, Vol. 8, No. 2, 1971, pp. 358–364.

[22]Markley, F. L., "Attitude Determination Using Vector Observations: A Fast Optimal Matrix Algorithm," *Journal of the Astronautical Sciences*, Vol. 41, No. 2, 1993, pp. 261–280.

[23]SODERN, "SED16 Star Tracker," URL: http://www.sodern.fr/SODERN/space/sensors/sed16.html [cited 31 March 2002].

[24]Junkins, J. L., and Turner, J. D., *Optimal Spacecraft Rotational Maneuvers*, Studies in Astronautics Series, Vol. 3, Elsevier, Amsterdam, 1986, pp. 23, 24.